**Highlighting a research article from the Kearney Lab at the University of Massachusetts Amherst and the Royal College of Surgeons in Ireland.**
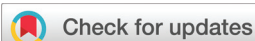
Development of wound healing scaffolds with precisely-triggered sequential release of therapeutic nanoparticles

This article describes the development of novel collagen-based tissue engineering scaffolds that have been functionalized with on-demand delivery system capable of releasing nanoparticles in response to ultrasound to coordinate regeneration.
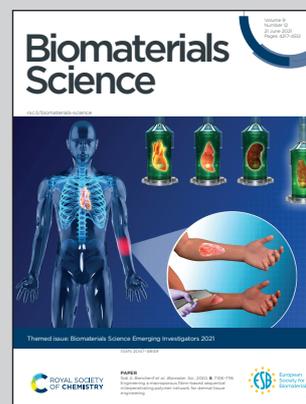
ROYAL SOCIETY OF **CHEMISTRY**

rsc.li/biomaterials-science

Check for updates

Development of wound healing scaffolds with precisely-triggered sequential release of therapeutic nanoparticles†

Tauseef Ahmad, [ID] [a] Sean McGrath, [a] Catherine Sirafim, [a]
Ronaldo J. F. C. do Amaral, [ID] [a] Shin-Loong Soong, [ID] [a] Renuka Sitram, [a]
Shifa'a Turkistani, [ID] [a] Francesco Santarella [ID] [a] and Cathal J. Kearney [ID] *[a,b,c,d]

Natural bioactive cue profiles are generally transient with cues switching on/off to coordinate successful outcomes. Dysregulation of these sequences typically leads to disease. Successful wound healing, for example, should progress sequentially through hemostasis, inflammation, granulation tissue formation, and maturation. Chronic wounds, such as diabetic foot ulcers, suffer from uncoordinated signaling, and arrest and cycle between the inflammation and granulation stages. Traditionally, therapeutic delivery in tissue engineering has focused on sustaining delivery of key signaling factors; however, temporal and sequential delivery have increasingly come into focus. To fully take advantage of these signaling systems, a scaffold or matrix material that can house the delivery system is desirable. In this work, we functionalized a collagen-based scaffold – which has proven regenerative potential in wounds – with on-demand delivery of nanoparticles. Building on our previous work with ultrasound-responsive alginate that shows near-zero baseline release and a rapid release in response to an ultrasound trigger, we developed two novel scaffolds. In the first version, homogeneously-distributed microparticles of alginate were incorporated within the collagen-glycosaminoglycan (GAG) scaffold; ultrasound-triggered release of platelet derived growth factor (PDGF) loaded gold nanoparticles was demonstrated; and their maintained bioactivity confirmed. In the second version, pockets of alginate that can be individually loaded and triggered with ultrasound, were incorporated. The ability to sequentially release multiple therapeutics within these scaffolds using ultrasound was successfully confirmed. These platforms offer a precise and versatile way to deliver therapeutic nanoparticles within a proven regenerative template, and can be used to deliver and probe timed therapeutic delivery in wound healing and other tissue engineering applications.

Introduction

The majority of biological processes follow carefully sequenced steps or stages (*e.g.*, protein synthesis, wound repair, fracture healing) and have timed signals that co-ordinate these sequences. When these sequences are dysregulated, pathology generally ensues. For example, tumor vasculature is associated with tortuous, disorganized vessels, and leakiness; this is attributed to its overabundance of vascular endothelial growth factor (VEGF) signaling.[1] By contrast, it has been shown that a strategy for blood vessel growth that delivers VEGF protein followed by a delayed delivery of platelet derived growth factor (PDGF) resulted in a more mature and developed structure *versus* either factor alone.[2,3] Another example is the persistent inflammation observed at chronic wound sites. The normal healing sequence is an early presence of pro-inflammatory 'M1' polarized macrophages and their subsequent reduction followed by a predominant presence of pro-repair 'M2' polarized macrophages;[4,5] this progression does not occur in chronic wounds. Successful wound healing is carefully sequenced: (I) hemostasis – blood clot formation; (II) inflammation – cells fight infection and remove debris; (III) granulation – fibroblasts lay down immature matrix and provide signaling to initiate epidermal regeneration and angiogenesis; (IV) remodeling – the matrix is matured. Chronic wounds, such as diabetic foot ulcers (DFUs), fail to progress through

[a]Tissue Engineering Research Group, Dept. of Anatomy and Regenerative Medicine, Royal College of Surgeons in Ireland (RCSI), Dublin, Ireland
[b]Advanced Materials and Bioengineering Research Centre (AMBER), RCSI and Trinity College Dublin, Dublin, Ireland
[c]Trinity Centre for Bioengineering, Trinity College Dublin, Dublin, Ireland
[d]Department of Biomedical Engineering, University of Massachusetts, Amherst, USA. E-mail: ckearney@umass.edu; Tel: +1 413-545-1073
†Electronic supplementary information (ESI) available. See DOI: 10.1039/d0bm01277g

this sequence. DFUs are complex skin wounds prevalent in 13% of American diabetics (6.3% globally) and an estimated 25% of all diabetics will suffer from a DFU in their lifetime.[6,7] These wounds are refractory to most treatments and, if they remain chronic, they have the devastating consequence of lower-leg amputation; globally, an amputation occurs every 30 seconds.[8] There are a diverse number of factors that contribute to the poor healing of DFUs, including vascular impairment, neuropathy, dysregulated inflammation, impaired growth factor production, and sub-optimal extracellular matrix deposition. The collective result is that DFUs have ineffective, unco-ordinated signaling and fail to progress through the normal wound healing cycle.[9]

These carefully sequenced biological events have motivated the investigation of drug delivery systems that move away from the traditional goal of sustained delivery,[10] and instead focus on sequential delivery to compliment natural sequences or direct the correct sequence.[11,12] On-demand delivery technologies are predicated on the fact that a change to the local drug delivery carrier can be triggered by an external signal (*e.g.*, light, ultrasound, magnetic field), which consequentially adjusts the drug release rate.[10–12] One of the earliest examples of an on-demand drug delivery system utilized ultrasound to destruct polymeric drug carriers to accelerate the release of drug payload.[13] Inspired by this work and work on sonophoresis[14] (whereby ultrasound reversibly enhances absorption through the skin), we previously developed an ultrasound-responsive alginate hydrogel for the on-demand delivery of small molecules, proteins, and nanoparticles.[15,16] In response to ultrasound, the release rate of small molecules – which have baseline diffusion from alginate – accelerates ~10-fold; due to the self-healing property of the ultrasound responsive alginate, when the ultrasound is stopped the release returns to baseline levels.[15] The effectiveness of this system was demonstrated both *in vitro* and *in vivo* for the delivery of a chemotherapeutic drug in a breast cancer model.[15] Incorporation of nanoparticles into the alginate – with sizes larger than the alginate pores (~10 nm) – further enhances control. As they are physically entrapped in the alginate hydrogel, baseline release is near-zero. These nanoparticles are then only released in response to ultrasound, with up to 5,000-fold increase in release rate demonstrated with ultrasound on *versus* off.[16] These systems allow for the precise delivery of particles that can be repeatedly dosed and due to the self-healing of the hydrogel, this system switches release off again in the absence of ultrasound. In modulating this system for complex tissue engineering cases, it will be most effective when used in conjunction with a tissue engineering scaffold.

A therapeutic strategy to stimulate healing at precise timepoints will be a key advantage; however, this still does not address two keys challenges in tissue engineering: maintaining the space (*i.e.*, preventing contraction or scar formation) where the regeneration is to occur, and providing the right extracellular environment. One of the earliest tissue engineering scaffolds – a porous collagen-glycosaminoglycan (CG) scaffold – disrupts scar formation and provides a template that fills the

space to be regenerated, facilitating cell attachment and generation of new tissue.[17] Many additional attempts to enhance wound healing have been explored since, including efforts to improve keratinization, such as an electrospun scaffold that mimics rete ridges to enhance epithelialization;[18] and donor tissue derived scaffolds, such as human amniotic membrane that promoted fibroblast growth and epithelialization.[19] A near-identical device to the original CG scaffold was approved in 2016 by the FDA for diabetic foot ulcers (Integra's Omnigraft®) and other clinically-approved DFU treatments (*e.g.*, Apligraf®) have collagen ECM as key precursor materials. Despite the proven regenerative potential of these scaffolds, to expedite healing or, in particular, to enhance healing in challenging wounds (*e.g.*, diabetic foot ulcers), instructing the host cells to step through the sequential phases of wound healing will be of great benefit. Clinical trials with Omnigraft® showed successful wound closure in 50% of patients.[20] This highlights its potential for healing DFUs; but also, the need for further functionalization to enhance healing. The previous demonstration of CG scaffolds as successful templates in skin wound healing motivates their use as a core regenerative scaffold. In broadening the applicability of the system, collagen-based scaffolds are additionally promising, as they have been adapted for a range of applications (*e.g.*, bone,[21] cartilage,[22] tendon,[23] nerve[24]). Additionally, collagen-based scaffolds have functionalized for sustained drug delivery.[25–28] Functionalizing these scaffolds with on-demand therapeutic delivery that orchestrates wound closure would provide an exciting new technical capability to tackle complex wounds.

In this work, we developed two different generations of on-demand delivery scaffolds (see Fig. 1). In the first, we have functionalized CG scaffolds with the ability to have homogeneously distributed on-demand microparticles throughout the scaffold, and confirmed the ability to release bioactive particles. To further enhance the functionality of this system, in the second generation, we incorporated individual pockets within the CG scaffold. These pockets can be individually triggered by ultrasound and stimulated to release nanoparticles sequentially from pockets. By developing this modular platform, it can be readily adapted to deliver a range of regenerative nanoparticles to mimic the body's natural repair processes, and the CG scaffold can also be separately modified to diversify the applicability of this system for other applications.

Results and discussion

Development of a CG scaffold with homogeneously distributed ultrasound-responsive microparticles

To develop the first generation of our on-demand scaffold system, we mimicked previously published protocols for homogeneous distribution of microparticles in collagen-based scaffolds (*e.g.*, ref. 26 and 25). First, model gold nanoparticles were generated following standard citrate reduction methods and coated with thiolated PEG to enhance stability. These particles were mixed with alginate and electrohydrodynamically
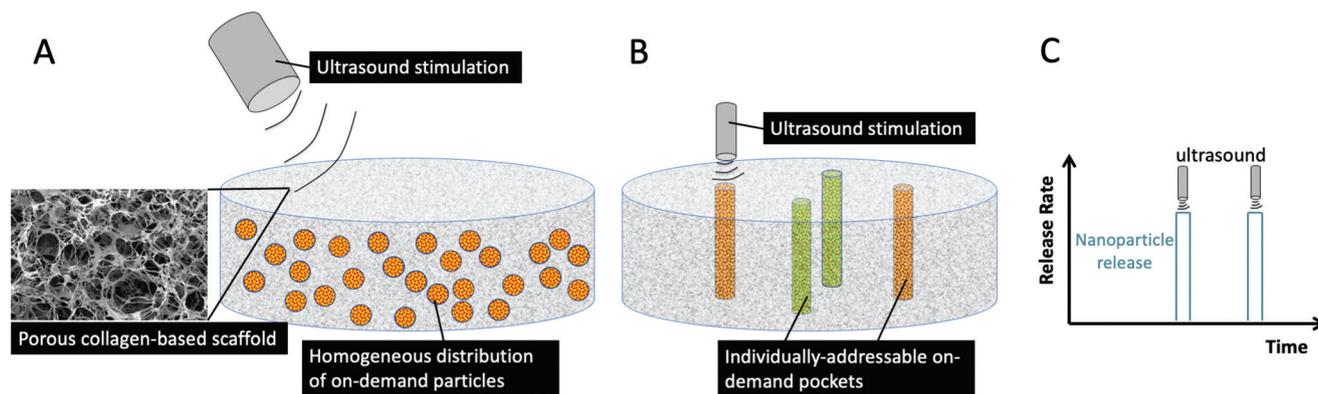
Fig. 1   Collagen-glycosaminoglycan scaffolds functionalized with on-demand nanoparticle delivery. (A) Microparticles of alginate capable of releasing nanoparticles in response to ultrasound are homogeneously distributed within a collagen-GAG (CG) scaffold. (B) In a second generation, alginate is incorporated in discrete pockets within the CG scaffold that can be individually loaded with different nanoparticles and triggered to release them at distinct timepoints. (C) Schematic of release profile in response to ultrasound.

sprayed to generate microparticles. Next, we modified standard fabrication techniques for CG scaffolds by adding an additional step to incorporate the microparticles, prior to freeze drying (see ESI Fig. 1†). Following formation of the standard collagen-GAG slurry, an additional 20% volume was added containing the ultrasound-responsive microparticles and rapidly mixed using luer lock syringes. The slurry and microparticles were then cast in stainless steel molds and processed in a freeze-dryer. Macroscopically, the resultant scaffolds had the standardly observed porous collagen architecture; however, red/wine spheres (indicative of gold nanoparticle loaded alginate microparticles; see Fig. 2A) were
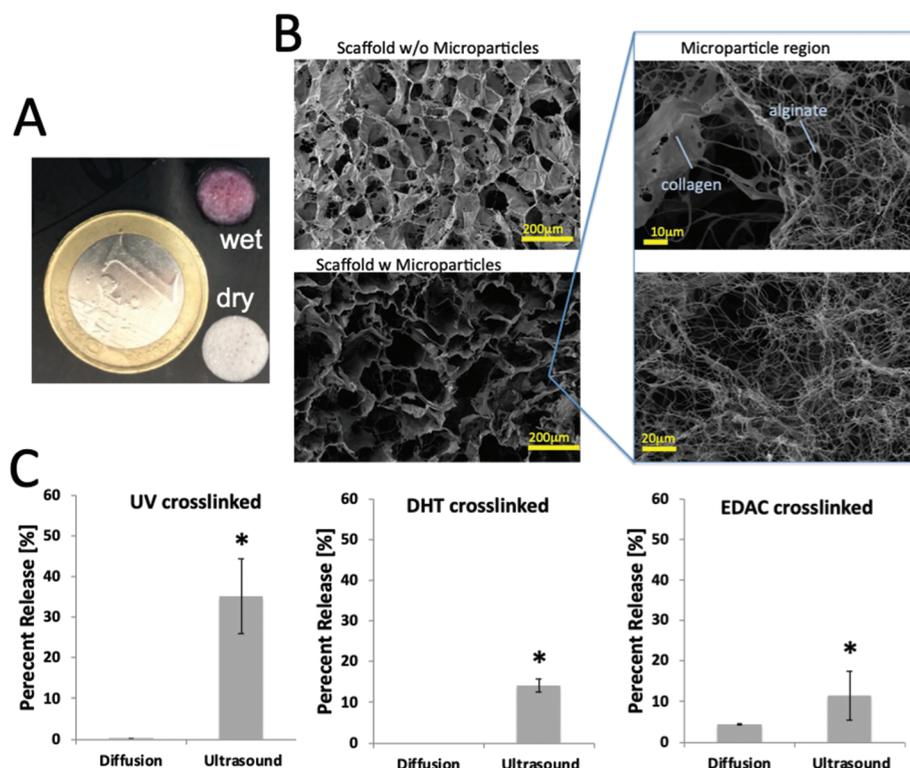

Fig. 2   Collagen-glycosaminoglycan scaffolds with homogeneously distributed on-demand delivery microparticles. (A) Photograph of wet and dry scaffolds following fabrication reveals the microbeads of alginate loaded with gold nanoparticles (which color the microparticles red/wine). (B) SEM imaging reveals a consistent pore structure between the scaffolds. Alginate microparticles can be identified within the scaffold. (C) Following cross-linking with UV, DHT, or EDAC, scaffolds had very low baseline diffusion. Treating the scaffolds with ultrasound (3 × 5 min, 25% amplitude, once per hour) resulted in a rapid release of nanoparticles (n = 3–4; error bars represent mean $\pm$ SEM; Student's t-test, *p < 0.05).

clearly visible and distributed throughout the scaffold. On SEM imaging, the porous architecture of the collagen scaffold was not disturbed when compared with control. Distributed within the pores were regions where alginate could be identified (see Fig. 2B).

Prior to ultrasound treatment, we screened three different crosslinking strategies for the CG scaffolds (in order of low to high crosslinking): ultraviolet,[29] dehydrothermal treatment, and EDAC crosslinking.[25] FTIR analysis confirmed amide bond formation for each of the crosslinking techniques and revealed no detectable differences in between samples irrespective of crosslinking method or inclusion of alginate microparticles (ESI Fig. 2†). These scaffolds were each treated with ultrasound (3×5 min, 25% amplitude, once per hour) and the release profile measured (see Fig. 2C). Whereas diffusion-release is negligible or zero, application of ultrasound successfully stimulated release of particles up to approximately 35%. Interestingly, we observed that as the collagen crosslinking was enhanced, there was a decrease in the quantity released in response to ultrasound. This was unexpected as the alginate microparticles should not be directly affected by the crosslinking; this crosslinking is designed to act on the collagen scaffold. Although there is previous evidence of a slight pore size reduction following EDAC crosslinking,[30] given the large pore size (>100 μm) relative to the nanoparticles used (~50 nm), this is expected to have only a minor effect on release; instead it is possible that reinforcing the collagen confers a protection on the alginate microparticles.

To assess whether the CG scaffolds alone could be used as an on-demand system, gold nanoparticles were directly incorporated into the CG slurry and freeze-dried. These scaffolds released negligible amounts of nanoparticles over the course of days, which suggested that the gold nanoparticles would only release in response to degradation of the scaffold. By applying ultrasound to UV-crosslinked scaffolds, a robust release of nanoparticles was observed (see ESI Fig. 2b†); however, this was associated with breakdown of the UV-crosslinked scaffold (see ESI Fig. 2c†). Interestingly, when EDAC crosslinked scaffolds with gold nanoparticles directly incorporated within them were treated with ultrasound, release of gold nanoparticles was observed. Thus, direct incorporation of gold nanoparticles into the CG scaffold may be an alternative approach that could be considered. Further work is required to confirm whether bioactive nanoparticles can be successfully incorporated and released using this approach.

For the alginate microparticle-loaded scaffolds, it was also noted that as collagen crosslinking was decreased, the scaffolds began to break up, with the UV scaffolds almost completely broken up by the ultrasound. These results conflict with what the project is aiming to design, *i.e.*, a high ultrasound release quantity with minimal degradation to collagen. To overcome this, in a second iteration of this homogeneously distributed scaffold, the two aspects of the device were separated into two layers, resulting in a bilayered scaffold design (see Fig. 3). In this bilayered scaffold design, the lower 'regenerative layer' is EDAC cross-linked and then, using a combi-
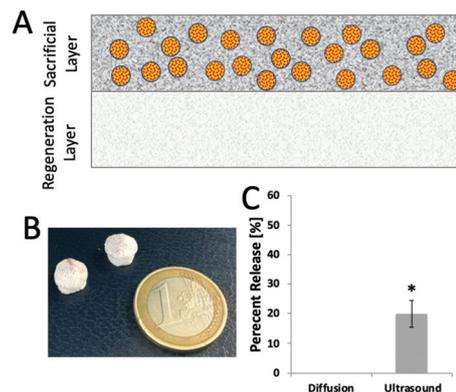

Fig. 3 Bilayered collagen-glycosaminoglycan scaffolds with a regenerative layer and a sacrificial therapeutic delivery layer. (A) Schematic overview of scaffold. (B) Photograph of scaffolds following fabrication reveals the individual layers and microbeads of alginate loaded with gold nanoparticles within the sacrificial layer. (C) Following crosslinking (EDAC in the regenerative layer, followed by UV when the sacrificial layer was added), no observable diffusion was recorded. Nanoparticles were successfully released in response to ultrasound (3×5 min, 25% amplitude, once per hour; $n = 3$; error bars represent mean $\pm$ SEM; Student's t-test, *$p < 0.05$).

nation of manufacturing techniques previously described[31,32] and the above fabrication processes, a second layer – the sacrificial drug delivery layer – is added on top. These scaffolds were successfully fabricated and the ability to release model nanoparticles from these scaffolds using ultrasound was successfully confirmed (see Fig. 3).

On-demand release of PDGF-functionalized gold nanoparticles from CG scaffolds

The monolayer and bilayer scaffold offer two options for on-demand release from homogeneously distributed microparticles within CG scaffolds. To confirm that this system could be used with a bioactive particle, we developed platelet derived growth factor (PDGF) coated gold nanoparticles. The applicability of PDGF for wound healing is evidenced by its previous clinical use for diabetic foot ulcers.[33] It is of additional interest in on-demand delivery systems as it is known to mature blood vessels, particularly when it is delivered at the right time.[2,3,34]

A range of strategies have been tested for attaching proteins to gold nanoparticles, with the simplest strategy taking advantage of cysteine residues in proteins forming thiol bonds with the gold surface.[16,35] Where stability is an issue, a hybrid method has been attempted, that covers some of the surface with PEG and leaves some available for protein attachment.[36] Alternatively, double thiol PEG can be coated on the gold nanoparticles, leaving available thiol groups to attach to the PDGF. We evaluated all three strategies, and measured the increase in hydrodynamic size of the particles, colloidal stability, and association efficiency of the PDGF (see Fig. 4). The PEG coatings added an additional 10–20 nm onto the hydrodynamic radius, with the PDGF only increasing the mPEG coated samples by a small amount (<10 nm) but the
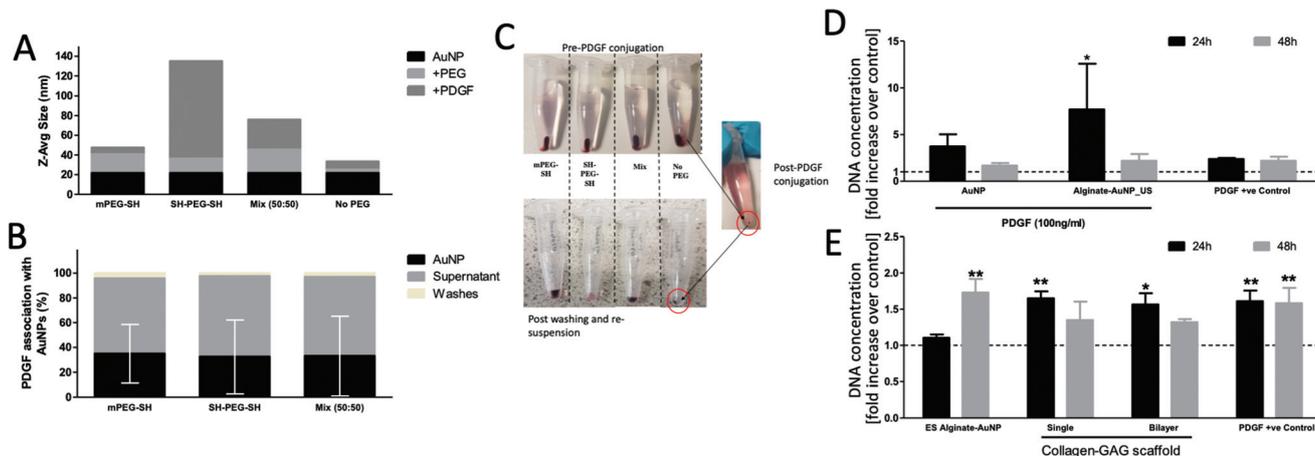
Fig. 4 Development, release, and bioactivity testing of PDGF-conjugated gold nanoparticles. (A) Change in hydrodynamic size of gold nanoparticles (AuNPs) following PEGylation and PDGF conjugation. AuNPs were incubated with different species of PEG (either mPEG, thiol-PEG-thiol, or 50 : 50 mix thereof) before being conjugated to PDGF. Changes in hydrodynamic size (nm) at each step were measured using a zetasizer. (B) Following conjugation reactions with PDGF, the supernatants and washes were assayed and the percentage of PDGF bound to AuNPs calculated subtractively ($n = 3$; error bars represent mean $\pm$ SEM). (C) Images of nanoparticles pre- and post-PDGF conjugation. The mPEG-SH group was most stable and selected for bioactivity studies. (D) hMSCs from different donors were incubated with PDGF, PDGF-AuNPs (AuNP) or PDGF-AuNPs released by ultrasound from alginate microspheres (Alginate_AuNP_US). (E) BJ fibroblasts were incubated with PDGF or PDGF-AuNPs released by ultrasound (US) from either alginate microspheres (ES Alginate_AuNP) or CG scaffolds (either single or bilayered). For (D) and (E), treatments were added at an effective PDGF concentration of 100 ng ml^{-1} for 24–48 hours and cellular DNA measured by PicoGreen. Data is presented as the fold increase in DNA content over untreated controls (broken horizontal line at $y = 1$) ($n = 3$–4; error bars represent mean $\pm$ SEM; 2-way ANOVA with Bonferonni *post-hoc*, *$p < 0.05$, **$p < 0.01$).

SH-PEG-SH samples dramatically (~100 nm). When no PEG was added to the nanoparticles, however, they were colloidally unstable and precipitated to the bottom of the microcentrifuge tubes following washing steps (see Fig. 4C). In contrast, the mPEG-SH/PDGF combination appeared to be the most stable and these were brought forward for further testing. The PDGF association efficiency – determined by subtractive ELISA – was approximately the same (~34%) for all three types of PEG combinations; however, the recorded variation was very large. Thus, we additionally directly estimated the association efficiency for mPEG-SH/PDGF nanoparticles by SDS-PAGE/silver staining and the association efficiency was determined to range between 38–71% (see ESI 3†). To bring forward the PDGF particles to bioactivity studies, from these two datasets, we estimated a value of 50% PDGF binding efficiency.

The bioactivity of these nanoparticles was then confirmed by incubating them with hMSCs and demonstrating enhanced proliferation per previous studies in our lab (ref. 37; see Fig. 4D). These studies confirmed that the coated AuNP – both freshly made, and following encapsulation and release from the microparticles – demonstrate a bioactive effect, consistent with previous work for BMP-2 coated nanoparticles in the system.[16]

To complete the development of the scaffold, we then incorporated these nanoparticles within our monolayer (EDAC crosslinked) and bilayered scaffolds, and stimulated them with ultrasound. The maintained bioactivity of these scaffolds was confirmed by incubating released nanoparticles with fibroblast cells (key cells in wound healing), with the single and bilayered

scaffold groups outperforming negative controls, and matching the PDGF positive control (see Fig. 4E). This data successfully demonstrated the ability to trigger release of bioactive particles from within a regenerative collagen-based scaffold. However, the homogeneous distribution of particles does not allow for individual triggering of therapeutics. This motivated the development of a second scaffold, with discrete alginate pockets that could be individually filled and triggered with ultrasound. Additionally, for the homogeneously distributed scaffold, all regions of the scaffold are required to be targeted by ultrasound, which can have adverse effects on cell viability and/or attachment. To test this, we applied ultrasound diffusely to scaffolds seeded with fibroblasts and measured cell content (see ESI Fig. 4†). Cell numbers in these scaffolds were reduced by up to 55% after three cycles of ultrasound. Although this is not desirable, the full deleterious effect of ultrasound needs to be assessed *in vivo* as the distribution of the ultrasound signal is different in a more homogeneous environment, especially as the pores fill with regenerated tissue (cells were only seeded for three days prior to ultrasound in these experiments and are unlikely to have generated sufficient extracellular matrix to be embedded within).

Development of a CG scaffold with individual pockets that can be triggered to release nanoparticles on demand

First, we designed stainless steel molds with posts on the base that protrude into the collagen slurry to yield a hollow pocket after the freeze-drying process (see Fig. 5). These scaffolds were crosslinked with DHT followed by EDAC. Next, we went
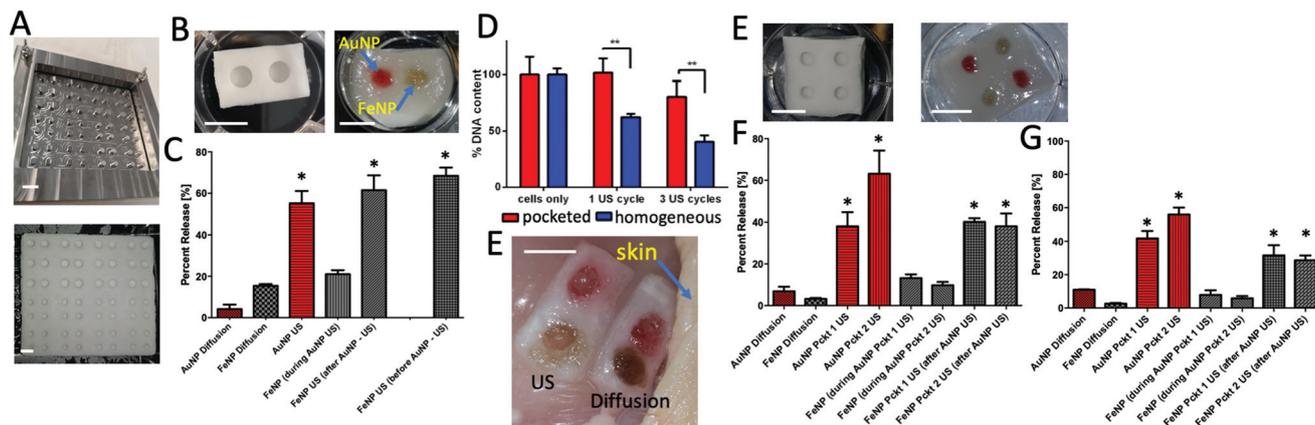
Fig. 5 Development and testing of collagen-GAG scaffolds with ultrasound-responsive alginate pockets. (A) Photographs of mold and resultant collagen-GAG scaffold following freeze-drying. (B) Collagen-GAG scaffold pre- (left) and post-crosslinking and alginate loading (right). Alginate loaded with gold nanoparticles (AuNP) has a red/wine color; alginate loaded with iron oxide nanoparticles has a grey/brown color. (C) Sequential release profiles from two-pocket scaffold with the AuNP pocket triggered first (left bars) or FeNP pocket triggered first (right bar). Release of FeNP during AuNP triggering was not significantly different to diffusion release. Following AuNP triggering, the FeNP were then successfully released by targeting the FeNP alginate pocket (n = 3–4; error bars represent mean $\pm$ SEM; one-way ANOVA (AuNP groups and FeNP groups compared individually) with Bonferonni *post-hoc* of all groups *versus* diffusion release only, *p < 0.05). (D) Bilayered scaffolds were placed under the skin of an *ex vivo* chicken thigh and triggered with ultrasound (left scaffold) or left untreated (right scaffold). (E) 4-Pocket collagen-GAG scaffold pre- (left) and post-crosslinking and alginate loading (right) with individual pockets loaded with alginate containing AuNP or FeNP. (F) and (G) Sequential release profiles from 4-pocket scaffolds with pockets (F) 2.5 mm deep, or (G) 3.5 mm deep. AuNP pockets were sequentially triggered ('AuNP Pckt 1, 2 US') – with non-significant changes in FeNP release ('FeNP (during AuNP Pckt 1, 2 US)') *versus* diffusion controls – followed by ultrasound triggering of FeNP pockets ('FeNP Pckt 1, 2 US (after AuNP US)') (n = 3–4; error bars represent mean $\pm$ SEM; one-way ANOVA (AuNP groups and FeNP groups compared individually) with Bonferonni *post-hoc* of all groups *versus* diffusion release only, *p < 0.05). Scale bar on (A), (B), (D) and (E) represents 10 mm.

through a series of iterations to identify a suitable injectable alginate formulation that could fill and remain within the scaffold pockets, without spreading into the surrounding parts of the scaffold (see ESI 5†). A two pocket and four pocket version of the scaffold was successfully fabricated and the pockets filled with alginate loaded with PEGylated gold nanoparticles (AuNP) or PEGylated iron nanoparticles (FeNP). Following successful fabrication of these scaffolds, baseline diffusion from the scaffolds remained low (<20%).

Beginning with the two-pocket scaffold (see Fig. 5C), the gold nanoparticles showed robust release in response to ultrasound treatment directed at that pocket (AuNP US). When compared with the diffusion release (FeNP diffusion), only a small additional amount of iron nanoparticles were released while the gold nanoparticle pocket was being stimulated ('FeNP (during AuNP US)'). However, when ultrasound was directed at the iron nanoparticle pocket, a robust response to ultrasound was observed ('FeNP (after AuNP US)'). The release value matched the value for when the iron nanoparticle pocket was struck first ('FeNP US (before AuNP US)').

Next, picoGreen was used to assess fibroblast cell numbers with or without ultrasound in these scaffolds, when the ultrasound trigger is directed at the alginate pocket only. Whereas the homogeneously distributed ultrasound signal reduced cell number, when the signal was directed at the pocket alone – in the same manner as in the release studies – no reduction in cell numbers was observed for up to three cycles (Fig. 5D and ESI Fig. 4†). To further assess whether this device is capable of translation *in vivo*, an *ex vivo* release experiment was con-

ducted using chicken thighs as previously described.[38] When the devices were placed under chicken skin and stimulated with ultrasound, there was a visual loss of color compared to the diffusion-only scaffold (indicating nanoparticle release), and some staining apparent in the scaffold area surrounding the pockets. To understand whether multiple pockets can be sequentially triggered, we next tested the release profile from a four-pocket scaffold, one with pockets 2.5 mm deep (Fig. 5F), and one with pockets 3.5 mm deep (Fig. 5G). For both scaffolds, both gold pockets released individually in response to ultrasound ('AuNP Pckt 1, 2 US'). During stimulation of the gold pockets, a small amount is released from the iron pockets, but this is consistent with the amount released from the diffusion-only control scaffolds (separate, non-stimulated scaffolds). Similar to the two-pocket scaffold, both iron nanoparticle pockets released sequentially in response to ultrasound stimulation.

This work develops two novel scaffolds and lays the foundation for *in vivo* studies that will first confirm the full therapeutic potential of the device, and secondly, enable the ability to explore the effect of therapeutic delivery timing – and sequential therapeutic delivery timing – on wound healing processes. In future work, the ability to release these nanoparticles *in vivo* and for them to have a therapeutic effect will be explored. Previous authors have successfully demonstrated the ability to stimulate release of therapeutics from within scaffolds using acoustic energy by making the drug carriers susceptible to different ultrasound levels.[39] Their system yielded a steady release from the embedded capsules over

several days following triggering, which is desirable for certain applications. The devices described here show a more abrupt release profile, which offers the advantage of having a precise timepoint as a tool to probe the timing of therapeutic delivery and their effect on biological processes. Future work will also refine the size and distribution of scaffold pockets and focusing of the ultrasound to ensure that sufficient nanoparticle dosing is delivered throughout the scaffold.

Conclusions

Herein, we successfully developed novel platform technologies for precisely-timed delivery of therapeutic nanoparticles. In the first system, where a single payload – or a single triggering event – is all that is required, fabrication of a collagen-GAG scaffold with homogeneously distributed microparticles was developed. The ability to incorporate and release bioactive nanoparticles on-demand from this system was then demonstrated. In the second system, discretized pockets within the scaffold can be individually triggered to release their payload on-demand, which allows for precise, sequential delivery of therapeutics within a scaffold. These tools show great promise for interrogating the optimum profile for carefully sequenced delivery of therapeutics to wound sites, and bring us closer to mimicking the exquisite temporal control observed in natural processes.

Materials and methods

AuNP synthesis, PEGylation, and PDGF coating

Core AuNPs were formed using standard citrate methods.[35] 400 mL of 98.5 mg mL^{-1} gold(III) chloride trihydrate (Sigma Aldrich, St Louis, MO) was stirred on a hotplate. 10 mL of a sodium citrate (Sigma Aldrich) solution (7.5 mg mL^{-1}) was rapidly added, leading to the formation of AuNPs of roughly 30 nm diameter. The solution was allowed to cool to room temperature before proceeding.

For PEGylation, 1 mM solution of methoxy-polyethylene glycol-thiol (mPEG-SH) and thiol-polyethylene glycol-thiol SH-PEG-SH (both MW = 5000 Da; Jenkem Technologies) was prepared and sterile filtered. Core AuNPs were sterile filtered (Steriflips) and mPEG-SH or SH-PEG-SH solution was added dropwise with stirring. PEGs were added at a ratio of 2.5 PEG ligands per nm^2 of AuNPs; mPEG-SH, SH-PEG-SH, or a 50 : 50 mixture of the two were added to AuNPs. Samples were agitated overnight at room temperature on an orbital shaker.

For PDGF coating, AuNP-PEG were aliquoted into 15 ml tubes and sterile filtered trehalose (Sigma T9449) solution (final concentration 100 mg mL^{-1}) was added. Recombinant human PDGF (1.61 ng ml^{-1}; rh220BB R&D) was added dropwise to a mix of AuNP-PEG/trehalose at a ratio of 1 ng PDGF per μg of AuNP-PEG, similar to previous authors.[36] The mixture was agitated overnight at room temperature on an orbital shaker. Particles were characterized followed by cen-

trifugation (13 000 rcf) to remove excess unbound PDGF and trehalose and washed with DI water 3 times. Supernatant and pooled washes were saved for analysis by ELISA. Washed nanoparticles were redispersed in sterile water for cell assays and silver staining. AuNPs with or without PEG and PDGF coating were characterised using a Zetasizer (Malvern).

PDGF quantification on nanoparticles using ELISA

Supernatants and pooled washes from PDGF conjugation reactions (see Methods section above) were analysed by enzyme linked immunosorbent assay (ELISA) to quantify the amount of unbound PDGF according to kit manufacturer's instructions (DY220, R&D systems). Direct quantification of PDGF bound to nanoparticles by ELISA did not yield reliable results as the nanoparticles could not be immobilized in ELISA plates for the assay. The amount of PDGF bound to nanoparticles was therefore deduced by a subtractive method (i.e., by analyzing washes and supernatant). Quantification by silver stain is described in ESI 2.†

Electrohydrodynamic spraying of alginate and incorporation of PDGF-AuNPs into electrosprayed alginate beads

Low molecular weight (LMW; Sigma Aldrich, Germany) and high molecular weight (HMW; (Pronova)) sodium alginate powder were dissolved in phosphate buffered saline (PBS) to form final concentration stock solutions of 2.5% and 2.0% respectively. These solutions were mixed with PDGF conjugated AuNPs 10 times in luer lock connected syringes to obtain a final 1% LMW:0.25%HMW alginate. The mixture was then sterile electrohydrodynamically sprayed at 250 μL min^{-1} with a 22G needle @18 kV into 100 mM CaCl$_2$ and crosslinked for 30 min. PDGF-AuNPs incorporated alginate microparticles thus obtained were washed with sterile water and stored in PBS (with Ca^{2+} ions) until used.

Fabrication of collagen-glycosaminoglycan scaffolds with microbeads

Collagen-GAG (CG) was prepared as previously described.[34,40] Briefly, microfibrillar type I bovine tendon collagen (Collagen Solutions Inc., Glasgow, UK) was blended with chondroitin-6-sulfate, isolated from shark cartilage (Sigma-Aldrich, Germany) in 0.05 M acetic acid. To prepare single layer alginate-PDGF-AuNP doped scaffolds, 4 parts CG slurry with 1 part alginate microparticles (with PDGF-AuNPs) was mixed using luer lock syringes and freeze dried (see ESI Fig. 1†). The suspension was cast in stainless steel molds and frozen to a final temperature of −10 °C, which was constantly maintained for 60 min, and then sublimated under vacuum (100 mTorr) at 0 °C for 17 h.[34,40] Cylindrical scaffolds were crosslinked by UV cross-linked @ 365 nm for 15 min; dehydrothermal treatment (DHT) using a vacuum oven (Vacucell, MMM Group, Munich, Germany) at 0.05 bar and 105 °C over 24 h; or chemically cross-linked (following DHT) using 1-ethyl-2-(3-dimethyl-aminopropyl) carbodiimide (EDAC) in combination with N-hydroxysuccinimide (NHS) as previously described. A PerkinElmer Spectrum 100 was used for collecting attenuated

total reflectance Fourier transform infrared (ATR-FTIR) spectra in the spectral region of 650–4000 cm^{-1}. To prepare collagen-gold nanoparticle scaffolds (without alginate beads), pegylated gold nanoparticles were added directly into the collagen-GAG slurry at the equivalent concentration to those incorporated in the alginate microbeads, in 1 part the volume in diH$_2$O to 4 parts collagen slurry.

To prepare bilayer scaffolds, the aforementioned procedure was first completed (without the addition of microbeads). These standard, EDAC crosslinked CG scaffolds served as base layers for preparing bilayered scaffolds. Next, 0.025 M acetic acid was added to the base layers spread in stainless steel molds. Excess acetic acid was removed and second layer of slurry (containing alginate microbeads) was added. This second (sacrificial) layer was prepared by mixing 3 parts standard CG slurry with 1 part alginate microparticles. Scaffolds were freeze dried as standard and UV cross-linked @ 365 nm for 15 min.

Ultrasound (US) treatment of Alginate-PDGF-AuNP microparticles and cell proliferation assays

In order to demonstrate their bioactivity, PDGF-AuNPs entrapped within alginate microparticles were released by application of US. PDGF-AuNPs-Alginate microparticles either alone or when incorporated within CG scaffolds (both single and bilayer) were suspended in 4.5 ml cell culture medium in 15 ml tubes. Ultrasound (Vibra-cell VCX 130 with 3 mm diameter probe, Sonics & Materials Inc., Newtown, USA) at an amplitude of 25% for 5 min was applied to PDGF-AuNPs-Alginate microparticles and was sufficient to fully release PDGF-AuNPs. For PDGF-AuNPs-Alginate microparticles incorporated within CG scaffolds, two US treatments were carried out: 25% amplitude for 5 min and 30% for 2.5 min to fully release the PDGF-AuNPs. Released PDGF-AuNPs from alginate were filtered through tissue mesh or sieves to remove alginate/CG debris. Alternatively, post-US mixture was centrifuged at 1200 rpm for 5 min and supernatants were collected for *in vitro* cell proliferation assays.

Human mesenchymal stromal cells (hMSC; p4-p6) ($n = 3$ different donors) were isolated from bone marrow aspirates obtained from the iliac crest of normal human donors 20–30 years old (Lonza Biologics PLC) or human BJ fibroblasts (p14–p20; gift from Garlick lab, Tufts university, Boston) were seeded in 24-well plates (20 000 cells per well). Treatments were applied two days after seeding in 300 μl per well for 24–48 hours. PDGF controls and PDGF-AuNPs released by US application were applied at an effective concentration of 100 ng ml^{-1}. In order to determine cell proliferation at each time point, treatments were removed and cells washed with warm PBS followed by cell lysis (sodium carbonate/Triton-X 100 lysis buffer). Cellular DNA content was quantified with Quant-iT PicoGreen dsDNA assay (Thermo Fisher Scientific, Biosciences, Ireland) according to manufacturer's instructions.

Formation of pocketed scaffolds

As described above for the monolayer scaffolds, a standard CG slurry was prepared, cast in modified molds, freeze-dried and crosslinked (DHT and EDAC). Next, the injectable alginate was prepared. 600 μL and 675 μL of HMW and LMW alginate stocks (8% w/v and 3% w/v, respectively) were loaded into a 3 mL luer-lock syringe. 375 μL of the AuNP stock (1.43 mg ml^{-1}) was pipetted into the same 3 mL luer-lock syringe. 75 μL of deionised water and 75 μL of 1.2 M Calcium Sulphate solution was added to a second 3 mL luer-lock syringe. Syringes were connected by luer locks and mixed. The final solution had concentrations of 3% LMW and 1% HMW alginate, 50 mM of Calcium Sulphate and 297.9 μg ml^{-1} of AuNP. PEGylated Iron oxide nanoparticles (FeNP, Sigma Aldrich, St Louis, MO) were similarly mixed, and had a final concentration of 175 μg ml^{-1} of FeNP. Note that PEGylated iron nanoparticles were used here as an additional model nanoparticle that could be independently measured, not for their magnetic properties.

Ultrasound release from pocketed scaffolds

Ultrasound release studies were performed in six-well plates with a sponge material placed on the base of each well. A two or four pocket collagen-GAG scaffold that had been both physically and chemically crosslinked was then pinned at diagonal corners to the base sponge material in each well (see ESI Fig. 4†). In this study, the two-pocket scaffold had a pocket diameter and depth of 6 mm and 2.5 mm respectively whilst the four-pocket scaffolds pockets had a diameter of 4 mm and depths of either 2.5 mm or 3.5 mm. The AuNP and FeNP loaded hydrogels that were freshly mixed, were then injected into each pocket until the pocket was full, and allowed to complete crosslinking for 40 minutes prior to the beginning of the release study. After 40 minutes had elapsed, 3 mL or 3.5 mL of PBS at room temperature was added to the well with to completely submerge the pocket scaffold. The tip of the ultrasound probe (Vibra-cell VCX 130 with 3 mm diameter probe) was then submerged into the PBS in alignment with one of the pockets on the scaffold whilst ensuring that the distance between the tip of the ultrasound probe and the pocket on the scaffold was at least 3 mm (see ESI Fig. 4†).

Each pocket was subjected to an ultrasound intensity of 25% for 2.5 minutes. The full 3 mL of PBS was withdrawn from the well between each ultrasound cycle and placed into a 5 mL tube before a fresh 3 mL of PBS was then added before commencing the next cycle. Control, diffusion samples were separate from the ultrasound samples, and run in parallel.

The standard curve for each nanoparticle was determined by doing serial dilutions of the stock solution of both the AuNPs, which had a concentration of 1.43 mg ml^{-1}, and the FeNPs, which had a concentration of 1 mg ml^{-1}. An iron colorimetric assay kit (Sigma Aldrich) was used to determine the amount of FeNPs released during the ultrasound release study. 100 μL samples were taken from each ultrasound release point in triplicate and added to a 96 clear well plate along with the serial dilutions of the stock solution and a control PBS sample. A spectrophotometer was used to measure the absorbance of the samples at a wavelength of 288 nm and 518 nm for the FeNPs and AuNPs respectively and these values were

related to the appropriate standard curve to determine the amount of the nanoparticles that been released during the ultrasound application.

Similar to methods described previously[41] scaffolds were placed under the skin of chicken thighs, from chicken carcass (Dunnes Stores, Ireland). Ultrasonic coupling gel was used to couple the US transducer to the skin and individual pockets of the scaffold were stimulated will ultrasound twice each.

Effect of ultrasound on cell numbers in scaffolds

BJ cells were seeded on the scaffolds at a density of 2000 cell per mm^3 and incubated for 30 min. To mimic ultrasound application in the homogeneous on-demand delivery scaffolds, scaffolds were incubated in 2 mL media for 3 days prior to ultrasound. For the pocketed scaffolds, agarose was added to the bottom of the wells to fix pocketed scaffolds in place prior to seeding. Empty alginate, with no therapeutic was incorporated in the pockets. Agarose was added on the sides of the scaffold to maintain it in place. After addition of 4.5 mL media, scaffolds were left to proliferate for 3 days. Ultrasound was applied as per release experiments, *i.e.*, in 5.5 ml media in conical tubes for 5 min 25% amplitude in a conical tube where the scaffold is free to move; or directed at the alginate pockets for the pocketed scaffold. Cells were lysed using a solution of 0.2 M sodium carbonate and 1% Triton X. DNA quantity was evaluated immediately afterwards by PicoGreen (QuantIt PicoGreen, Invitogen) according to manufacturer's protocol.

Statistics and analysis

Graphs express averages ± standard error mean (SEM) and $n = 3$ at a minimum was used in all experiments. For 2 sample comparison, Student's t-test was employed. One- or two-way ANOVA with Bonferroni or Tukey's *post-hoc* testing was used to analyze multiple-comparison datasets. Results were considered significant when $p < 0.05$ and indicated on the graphs as *. Complete details are described in the figure legends.

Conflicts of interest

The authors have no conflicts of interest to disclose.

Acknowledgements

References

1 P. Carmeliet and R. K. Jain, Angiogenesis in cancer and other diseases, *Nature*, 2000, **407**, 249–257.

2 R. R. Chen, E. A. Silva, W. W. Yuen and D. J. Mooney, Spatio-temporal VEGF and PDGF delivery patterns blood vessel formation and maturation, *Pharm. Res.*, 2007, **24**(2), 258–264.

3 T. P. Richardson, M. C. Peters, A. B. Ennett and D. J. Mooney, Polymeric system for dual growth factor delivery, *Nat. Biotechnol.*, 2001, **19**(11), 1029–1034.

4 M. P. Rodero and K. Khosrotehrani, Skin wound healing modulation by macrophages, *Int. J. Clin. Exp. Pathol.*, 2010, **3**(7), 643–653.

5 R. Sridharan, A. R. Cameron, D. J. Kelly, C. J. Kearney and F. J. O'Brien, Biomaterial based modulation of macrophage polarization: A review and suggested design principles, *Mater. Today*, 2015, **18**(6), 313–325.

6 J. B. Rice, U. Desai, A. K. G. Cummings, H. G. Birnbaum, M. Skornicki and N. B. Parsons, Burden of diabetic foot ulcers for medicare and private insurers, *Diabetes Care*, 2014, **37**(3), 651–658.

7 P. Zhang, J. Lu, Y. Jing, S. Tang, D. Zhu and Y. Bi, Global epidemiology of diabetic foot ulceration: a systematic review and meta-analysis†, *Ann. Med.*, 2017, **49**, 106–116.

8 A. Raghav, Z. A. Khan, R. K. Labala, J. Ahmad, S. Noor and B. K. Mishra, Financial burden of diabetic foot ulcers to world: a progressive topic to discuss always, *Ther. Adv. Endocrinol. Metab.*, 2018, **9**, 29–31.

9 S. Noor, M. Zubair and J. Ahmad, Diabetic foot ulcer - A review on pathophysiology, classification and microbial etiology, *Diabetes Metab. Syndr.*, 2015, **9**(3), 192–199.

10 C. J. Kearney and D. J. Mooney, Macroscale delivery systems for molecular and cellular payloads, *Nat. Mater.*, 2013, **12**(11), 1004–1017.

11 M. Mehta, K. Schmidt-Bleek, G. N. Duda and D. J. Mooney, Biomaterial delivery of morphogens to mimic the natural healing cascade in bone, *Adv. Drug Delivery Rev.*, 2012, **64**, 1257–1276.

12 Y. Brudno and D. J. Mooney, On-demand drug delivery from local depots, *J. Controlled Release*, 2015, **219**, 8–17.

13 J. Kost, K. Leong and R. Langer, Ultrasound-enhanced polymer degradation and release of incorporated substances, *Proc. Natl. Acad. Sci. U. S. A.*, 1989, **86**(20), 7663–7666.

14 S. Mitragotri, D. A. Edwards, D. Blankschtein and R. Langer, A Mechanistic Study of Ultrasonically–Enhanced Transdermal Drug Delivery, *J. Pharm. Sci.*, 1995, **84**(6), 697–706.

15 N. Huebsch, C. J. Kearney, X. Zhao, J. Kim, C. A. Cezar, Z. Suo, *et al.*, Ultrasound-triggered disruption and self-healing of reversibly cross-linked hydrogels for drug delivery and enhanced chemotherapy, *Proc. Natl. Acad. Sci. U. S. A.*, 2014, **111**(27), 9762–9767.

16 C. J. Kearney, H. Skaat, S. M. Kennedy, J. Hu, M. Darnell, T. M. Raimondo, *et al.*, Switchable Release of Entrapped Nanoparticles from Alginate Hydrogels, *Adv. Healthcare Mater.*, 2015, **4**(11), 1634–1639.

17 I. V. Yannas, J. F. Burke, D. P. Orgill and E. M. Skrabut, Wound tissue can utilize a polymeric template to synthesize a functional extension of skin, *Science*, 1982, **215**(4529), 174–176.

18 I. O. Asencio, S. Mittar, C. Sherborne, A. Raza, F. Claeyssens and S. MacNeil, A methodology for the production of microfabricated electrospun membranes for the creation of new skin regeneration models, *J. Tissue Eng.*, 2018, **9**, 1–8.

19 S. John, M. R. Kesting, P. Paulitschke, M. Stöckelhuber and A. von Bomhard, Development of a tissue-engineered skin substitute on a base of human amniotic membrane, *J. Tissue Eng.*, 2019, **10**, 1–14.

20 V. R. Driver, L. A. Lavery, A. M. Reyzelman, T. G. Dutra, C. R. Dove, S. V. Kotsis, H. M. Kim and K. C. Chung, A clinical trial of Integra Template for diabetic foot ulcer treatment, *Wound Repair Regen.*, 2015, **23**(6), 891–900.

21 J. P. Gleeson, N. A. Plunkett and F. J. O'Brien, Addition of hydroxyapatite improves stiffness, interconnectivity and osteogenic potential of a highly porous collagen-based scaffold for bone tissue regeneration, *Eur. Cells Mater.*, 2010, **20**(0), 218–230.

22 B. A. Harley, A. K. Lynn, Z. Wissner-Gross, W. Bonfield, I. V. Yannas and L. J. Gibson, Design of a multiphase osteochondral scaffold III: Fabrication of layered scaffolds with continuous interfaces, *J. Biomed. Mater. Res., Part A*, 2009, **92**(3), 1078–1093.

23 S. R. Caliari, M. A. Ramirez and B. A. C. Harley, The development of collagen-GAG scaffold-membrane composites for tendon tissue engineering, *Biomaterials*, 2011, **32**(34), 8990–8998.

24 L. J. Chamberlain, I. V. Yannas, H. Hsu, G. R. Strichartz and M. Spector, Near–terminus axonal structure and function following rat sciatic nerve regeneration through a collagen–GAG matrix in a ten–millimeter gap, *J. Neurosci. Res.*, 2000, **60**(5), 666–677.

25 E. J. Ryan, A. J. Ryan, A. González-Vázquez, A. Philippart, F. E. Ciraldo, C. Hobbs, *et al.*, Collagen scaffolds functionalised with copper-eluting bioactive glass reduce infection and enhance osteogenesis and angiogenesis both in vitro and in vivo, *Biomaterials*, 2019, **197**, 405–416.

26 E. Quinlan, A. López-Noriega, E. M. Thompson, A. Hibbitts, S. A. Cryan and F. J. O'Brien, Controlled release of vascular endothelial growth factor from spray-dried alginate microparticles in collagen–hydroxyapatite scaffolds for promoting vascularization and bone repair, *J. Tissue Eng. Regener. Med.*, 2017, **11**(4), 1097–1109.

27 S. R. Caliari and B. A. C. Harley, The effect of anisotropic collagen-GAG scaffolds and growth factor supplementation on tendon cell recruitment, alignment, and metabolic activity, *Biomaterials*, 2011, **32**(23), 5330–5340.

28 R. M. Capito and M. Spector, Collagen scaffolds for non-viral IGF-1 gene delivery in articular cartilage tissue engineering, *Gene Ther.*, 2007, **14**(9), 721–732.

29 N. Davidenko, D. V. Bax, C. F. Schuster, R. W. Farndale, S. W. Hamaia, S. M. Best, *et al.*, Optimisation of UV irradiation as a binding site conserving method for crosslinking collagen-based scaffolds, *J. Mater. Sci. Mater. Med.*, 2016, **27**(1), 1–17.

30 M. McKegney, I. Taggart and M. H. Grant, The influence of crosslinking agents and diamines on the pore size, morphology and the biological stability of collagen sponges and their effect on cell penetration through the sponge matrix, *J. Mater. Sci. Mater. Med.*, 2001, **12**(9), 833–844.

31 T. J. Levingstone, A. Matsiko, G. R. Dickson, F. J. O'Brien and J. P. Gleeson, A biomimetic multi-layered collagen-based scaffold for osteochondral repair, *Acta Biomater.*, 2014, **10**(5), 1996–2004.

32 C. O'Leary, B. Cavanagh, R. E. Unger, C. J. Kirkpatrick, S. O'Dea, F. J. O'Brien, *et al.*, The development of a tissue-engineered tracheobronchial epithelial model using a bilayered collagen-hyaluronate scaffold, *Biomaterials*, 2016, **85**, 111–127.

33 J. W. Park, S. R. Hwang and I. S. Yoon, Advanced Growth Factor Delivery Systems in Wound Management and Skin Regeneration, *Molecules*, 2017, **22**(8), 1–20.

34 R. J. F. C. do Amaral, B. Cavanagh, F. J. O'Brien and C. J. Kearney, Platelet-derived growth factor stabilises vascularisation in collagen–glycosaminoglycan scaffolds in vitro, *J. Tissue Eng. Regener. Med.*, 2019, **13**(2), 261–273.

35 J. Kim, L. Cao, D. Shvartsman, E. A. Silva and D. J. Mooney, Targeted delivery of nanoparticles to ischemic muscle for imaging and therapeutic angiogenesis, *Nano Lett.*, 2011, **11**(2), 694–700.

36 T. M. Raimondo and D. J. Mooney, Functional muscle recovery with nanoparticle-directed M2 macrophage polarization in mice, *Proc. Natl. Acad. Sci. U. S. A.*, 2018, **115**(42), 10648–10653.

37 R. J. F. C. do Amaral, N. M. A. Zayed, E. I. Pascu, B. Cavanagh, C. Hobbs, F. Santarella, *et al.*, Functionalising Collagen-Based Scaffolds With Platelet-Rich Plasma for Enhanced Skin Wound Healing Potential, *Front. Bioeng. Biotechnol.*, 2019, **7**, 371.

38 S. Kennedy, J. Hu, C. Kearney, H. Skaat, L. Gu, M. Gentili, *et al.*, Sequential release of nanoparticle payloads from ultrasonically burstable capsules, *Biomaterials*, 2016, **75**, 91–101.

39 A. Moncion, M. Lin, O. D. Kripfgans, R. T. Franceschi, A. J. Putnam and M. L. Fabiilli, Sequential Payload Release from Acoustically-Responsive Scaffolds Using Focused Ultrasound, *Ultrasound Med. Biol.*, 2018, **44**(11), 2323–2335.

40 C. M. Murphy, M. G. Haugh and F. J. O'Brien, The effect of mean pore size on cell attachment, proliferation and migration in collagen-glycosaminoglycan scaffolds for bone tissue engineering, *Biomaterials*, 2010, **31**(3), 461–466.

41 S. Kennedy, J. Hu, C. Kearney, H. Skaat, L. Gu, M. Gentili, *et al.*, Sequential release of nanoparticle payloads from ultrasonically burstable capsules, *Biomaterials*, 2016, **75**, 91–101.

This journal is © The Royal Society of Chemistry 2021